Investigation of turbulence rotation in limiter plasmas at W7-X with a new installed Poloidal Correlation Reflectometry

A. Krämer-Flecken[1], T. Windisch[2], W. Behr[3], G. Czymek[1], P. Drews[1], G. Fuchert[2], J. Geiger[2], O. Grulke[2], M. Hirsch[2], M. Knaup[1], Y. Liang[1], O. Neubauer[1], E. Pasch[2] and the W7-X Team[2]

[1]Institut für Energieforschung und Klimaforschung / Plasmaphysik, Forschungszentrum Jülich, 52425 Jülich, Germany
[2]Max Planck Institut für Plasmaphysik, 17491 Greifswald, Germany
[3]Zentralinstitut für Engineering, Forschungszentrum Jülich, 52425 Jülich, Germany

Corresponding Author: a.kraemer-flecken@fz-juelich.de

Abstract:
For the first operation phase of the optimized stellarator W7-X, a heterodyn Poloidal Correlation Reflectometry (PCR) diagnostic is installed and put into operation. The system is intended to measure the perpendicular (with respect to the magnetic field) turbulence rotation and turbulence properties as the correlation time and correlation length in the plasma edge. Furthermore, it is capable to give information on the magnetic field line pitch. Therefore the system consists of an array of microwave antenna distributed in poloidal and toroidal direction. The frequency range of 22 GHz to 40 GHz allows to access local plasma densities from $0.6 \times 10^{19}\,\mathrm{m}^{-3}$ to $2.0 \times 10^{19}\,\mathrm{m}^{-3}$.
During the first operation phase the turbulence rotation bas been measured. In addition the radial electric field is estimated and compared to neoclassical theory. The relatively low plasma density allows to cover 80% of the plasma radius. The obtained data cover various experimental programs and are partly presented in the paper.

1 Introduction

For many questions on transport in fusion plasmas the knowledge of the plasma velocity ($v_\perp$) perpendicular to B is of outstanding importance. From the velocity profile along the radius regions of strong velocity shear can be detected. Furthermore, velocity oscillations in the plasma edge yield information on zonal flows and geodesic acoustic modes. Both phenomena are believed to interact with small scale turbulence and hamper the radial transport. An overview on both phenomena and related experiments can be found in [1]. In addition these phenomena play an important role in the transition from L- to H-mode regimes. A lot of studies in the transitional phase are performed to understand the velocity shear and role of mesoscale structures [2] in the transition from L- to H-mode

in stellarators [3]. These studies are based on the knowledge of the mean perpendicular velocity and its fluctuations. Both can be accessed by a PCR diagnostic.
Under the assumption that the measured turbulence velocity has a negligible phase velocity with respect to the plasma rotation the radial electric field (E_r) is accessible. This quantity is of high importance for theoretical models on neoclassical transport in plasmas. But, also studies of the turbulent structure itself are of interest. With the information on the turbulent structures in the frequency domain and their dependence on global plasma parameter the measured turbulent structures can be attributed to certain plasma instabilities as ion temperature gradient (ITG)- or trapped electron (TEM) modes. These issues will be addressed in the next campaign at W7-X. To investigate the topics mentioned above, necessary experimental information on mean quantities like ($v_\perp, E_r$) and fluctuating quantities as well as the spectral distribution of turbulent structures in the frequency domain can be retrieved from poloidal correlation (PCR) diagnostics.
The paper discusses the design of a PCR diagnostic on W7-X and its commissioning in section 2. After a short introduction in the applied methodology in section 3 an overview of the first $v_\perp$- and E_r-measurements is given in section 4. The main achievements are summarized in section 5.

2 Design issues of the PCR system at W7-X

The PCR system at W7-X is thought to be operated at the interface between plasma core and edge physics [4]. It is installed in the highly elongated bean shaped plan at $\phi = 72°$ (AEA21) port. This port hosts a Doppler reflectometer and the PCR system. The PCR system is located slightly below the equatorial plane. The coordinates

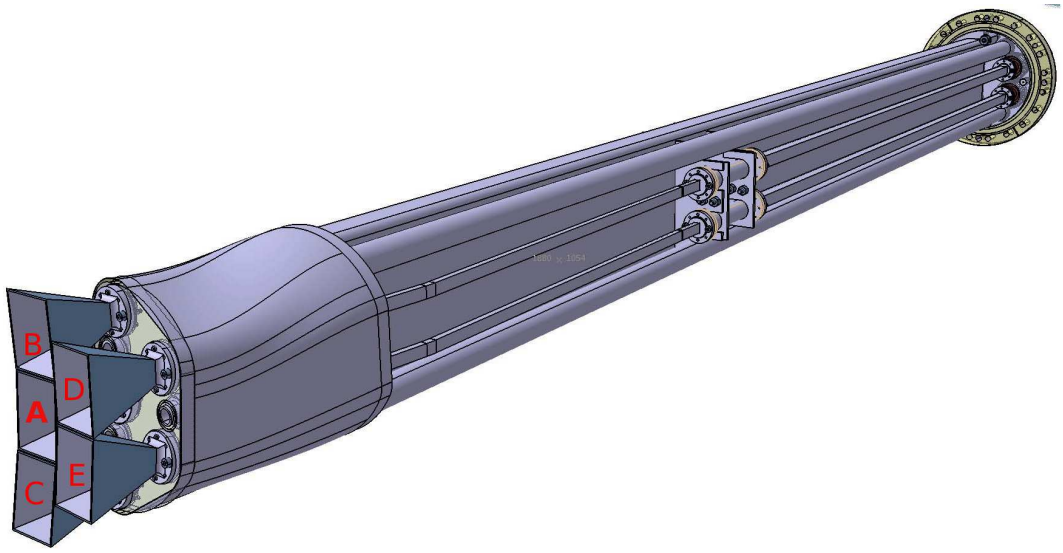

FIG. 1: Plugin of the PCR diagnostic with the notation of the horns by capital letters.

of the flange center are: $R = 8.102\,\mathrm{m}$, $\phi = 71.09°$ and $z = -0.16\,\mathrm{m}$. The system is

mounted from the outside and constructed in a way that the whole plugin can be installed from the DN 150CF. The flange hosts 5 microwave feed throughs, followed by a 1.5 m long wave guide connected to the antenna (see fig 1). The antenna labelled with letters B,C,D,E are receiving horns, the middle antenna in the first row is the launching horn (A). All five horns aim on the same focal point at $R = 6.0\,\mathrm{m}$, $\phi = 71.05°$ and $z = -0.104\,\mathrm{m}$. Each horn has a length of $l = 61\,\mathrm{mm}$ and the antenna opening is $44.1\,\mathrm{mm} \times 34.8\,\mathrm{mm}$. The antenna pattern has a 3 dB width of 14° in the H-plane. The whole antenna array is aiming upwards and has a certain angle with respect to the normal vector of the flux surface, obtained from the VMEC equilibrium calculations. For the case of geometrical optics the condition for reflection for each receiving antenna is calculated on a fine grid centred around the intersection point of the launcher with each flux surface. The grid size is 120 millimeter × 0.6 rad in z- and ϕ-direction, respectively. From the scalar product the angle between the reflected beam and the connecting line to each receiver is calculated for each grid point (see fig 2 for the case of antenna AC). Note the position fulfilling the reflection condition does not necessarily coincide with the line of sight (LoS) of the antenna. In all cases the minimum angle is found for slightly larger toroidal positions and slightly above the LoS of the antenna combination. Therefore a broad radiation pattern of the antenna is necessary.

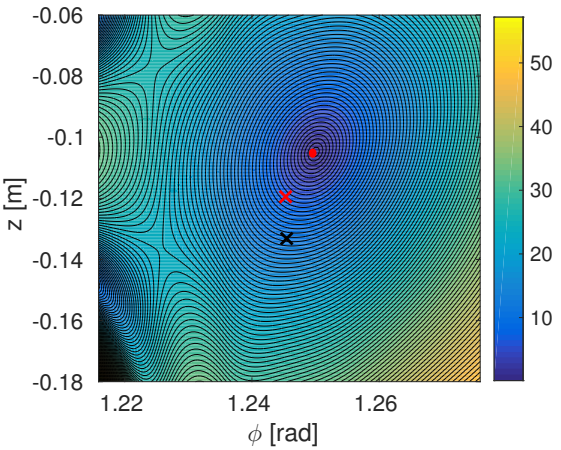

FIG. 2: Colour coded angle between reflected beam and LoS of the receiver for all grid points. Point of reflection is marked by red circle. The intersection of the launcher (red) and the receiver (black) cross is shown, too.

The reflectometer itself consists of two programmable microwave synthesizer coupled by a PLL. The frequency of the two synthesizers are off by 60 MHz which is the intermediate frequency of the system. The system operates in O-mode polarization which allows to cover a range of local densities ranging from $0.6 \times 10^{19}\,\mathrm{m}^{-3}$ to $2.0 \times 10^{19}\,\mathrm{m}^{-3}$. The phase fluctuations from the reflection layer of each receiving antenna are measured by a quadrature detector and sampled at 4 MHz.

3 Methodology

After identifying the frequency range of interest from cross phase and/or coherence spectra and adequate filtering of the raw data the cross correlation function for all 6 receiver combinations is calculated. The maximum of the cross correlation determined as:

$$\Delta t = \arg\max_t((|\ Y_i \star Y_j\ |)(t)) \tag{1}$$

where Y_i, Y_j denote the time series of the fluctuations from receiver i and j. The delay time (Δt) is the time it takes for a structure to propagate along the reflection layer from one receiver to the other. In fig 3 the cross correlation for all 6 combinations is shown. As expected with increasing Δt the cross correlation decreases. Two facts are of interest: (i) the difference in Δt for combinations with equal distance e.g. **BD**,**EC** in fig. 1 and (ii) the exponential decay of the cross correlation as function of Δt. The latter allows to estimate the decorrelation time of the structure (turbulence). The different Δt for equal z results from the inclination of the magnetic field lines in front of the antenna and allows to estimate the magnetic field line pitch [5] as:

$$tan(\alpha) = \frac{\Delta t_{BD} \cdot z_{EC} - \Delta t_{EC} \cdot z_{BD}}{\Delta t_{EC} \cdot s_{BD} + \Delta t_{BD} \cdot s_{EC}}, \tag{2}$$

where s, z denote the toroidal distance and the separation in z direction for a given antenna combination and the subscripts in capital letters denote the used antenna configurations. The distances for all receiver combinations in z- and toroidal direction are obtained from the point of reflection of the launcher-receiver combinations. In fig. 4 Δz distances are shown for all combinations as function of $r_{eff} = a_{LCFS}\sqrt{s}$, with $a_{LCFS} = 0.49\,\mathrm{m}$. For the

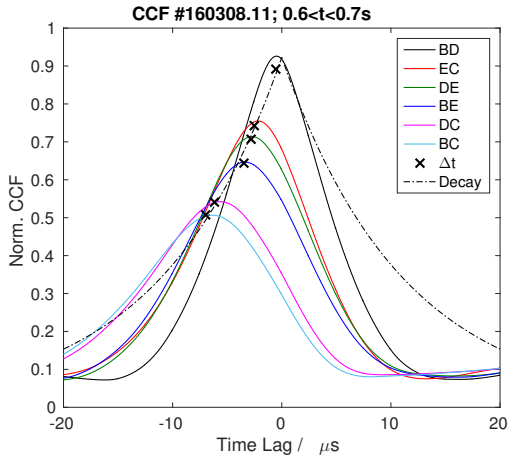

FIG. 3: The CCF as function of the time lag for all antenna combinations. Crosses denote the position of the fitted Gaussians. The dashed line describes the decay of the structure.

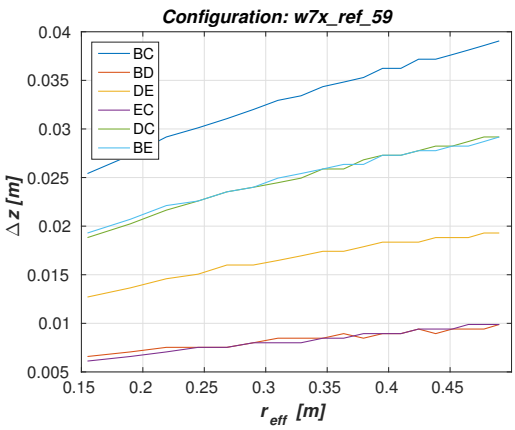

FIG. 4: Distance between the all receiver combination in z direction as function of r_{eff}

six combinations, the projection of the distances along $B_\perp$ and the Δt-values, a 1^{st} order polynomial is applied whose slope yields the turbulence rotation ($v_\perp$). The effect of the turbulence on the Δt estimation for the mean velocity is small ($\approx 10\,\%$) and is neglected here. Because information on the turbulence velocity with respect to the $E \times B$ velocity is missing, turbulence- and $E \times B$ velocity are assumed to be equal. This is justified because in case of mainly ITG turbulence the phase velocity is small compared to $E \times B$ velocity and can be neglected. It allows to estimate the radial electric of the plasma field as:

$$E_r = v_\perp \cdot B_\phi \tag{3}$$

4 First velocity measurements

The system has been operated during the full OP1.1 campaign. During December 2015 and January 2016 the duration of the plasma discharge was pretty short and used for commissioning of the diagnostic. However, in February and March the discharge duration improved considerable and first systematic studies became possible. At first the direction of the rotation is investigated. With respect to the antenna array the plasma rotates from bottom to top, counter clockwise, within the last closed flux surface. In the following the rotation profiles for different plasma scenarios are described. If not mentioned otherwise the raw data of each receiver is filtered in the range $5\,\mathrm{kHz} \leq f \leq 350\,\mathrm{kHz}$.

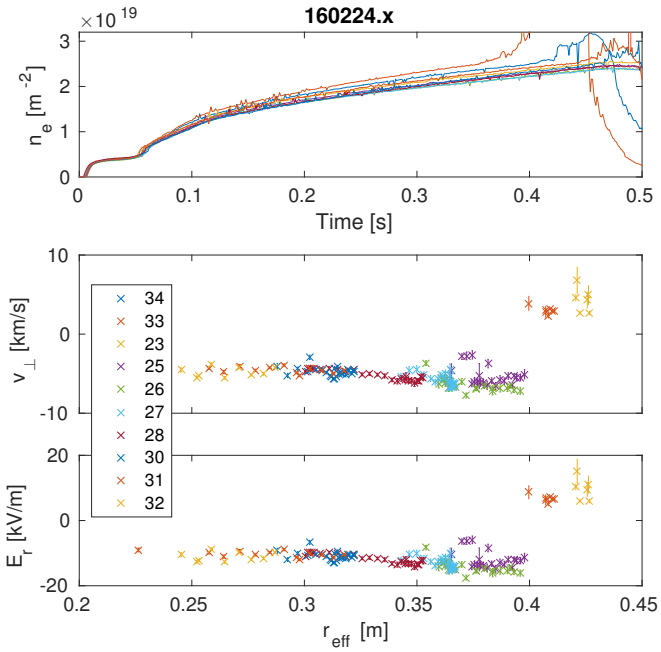

FIG. 5: Line averaged density (a) of a series of discharges. The $v_\perp$ and related E_r as function of r_{eff}. The different colours indicate the different discharges. Note the change in sign at the plasma edge.

4.1 Velocity profile measurements

A series of 10 plasma discharges each with a total heating power of $P_{ECRH} = 3.3\,\mathrm{MW}$ for a duration of $t = 450\,\mathrm{ms}$ is investigated. The frequency of the reflectometer is varied on a shot to shot basis. The line averaged density from interferometer measurements (see fig. 5a) is similar for all plasmas and slightly rising, reaching at the end of the ECRH pulse $\bar{n}_e = 2.5 \times 10^{19}\,\mathrm{m}^{-2}$. During the discharge the reflection layer moves towards the plasma edge as the frequency of the reflectometer is kept constant. With the density profile data from Thomson scattering [6], the position of the reflection layer is determined. The profile itself is approximated by $n_e(r) = n_0 \cdot (1 - (r/a)^p)^q$, where n_0 denotes the central plasma density. The calculated $v_\perp$ is shown in fig. 5b. The rotation profile is flat and increases slightly towards the plasma center. At the plasma edge (last closed flux surface) a transition towards positive $v_\perp$ is obtained. The transition is abrupt and the absolute values of $v_\perp$ in the plasma core and the edge are similar. The related E_r (see fig. 5c) yields values in the range $-12\,\mathrm{kV\,m^{-1}}$ to $-17\,\mathrm{kV\,m^{-1}}$ and shows a similar jump as $v_\perp$ at $r_{eff} \approx 0.4$.
At the plasma edge around the last closed flux surface the estimated $v_\perp$ and E_r can be compared with those values of the fast manipulator. A good agreement between both diagnostic is found which increases the confidence in both diagnostics [7].

4.2 Rotation in CERC plasmas

One of the main tasks within OP1.1 with its restricted set of diagnostic, was the search for core electron root confinement (CERC) regimes at W7-X. This regime is characterized by peaked electron temperature profiles and large positive radial electric field in the plasma center [8]. For plasmas with low electron density the PCR system is capable to measure deep in the plasma and should find evidence for a transition in the CERC regime. The analysed CERC discharges [9] exhibit certain densities and heating power scenarios. The ECRH power varies from 1.9 MW ($0\,\mathrm{s} \leq t \leq 0.4\,\mathrm{s}$) to 0.6 MW ($0.4\,\mathrm{s} \leq t \leq 0.7\,\mathrm{s}$) and jumps back again to 1.3 MW for $0.7\,\mathrm{s} \leq t \leq 1.0\,\mathrm{s}$. The PCR system is operated in a frequency scanning and a fixed frequency modus. For all CERC plasmas $v_\perp$ and E_r are calculated and shown in fig. 6a,b. From neoclassic analysis a positive E_r is expected for $r_{eff} \leq 0.2$. The PCR diagnostic in these plasmas accesses a range $r_{eff} \geq 0.25$. Furthermore those measurements are performed where the density profile becomes flat and the density scale length increases. Therefore the radial resolution of the PCR increases, too. Nevertheless for $r_{eff} \geq 0.25$ the absolute E_r is in fair agreement with measurements of a x-ray imaging crystal spectrometer as well as calculations [10]. Also the dip position in the E_r profile at $r_{eff} \approx 0.3$ is reproduced.

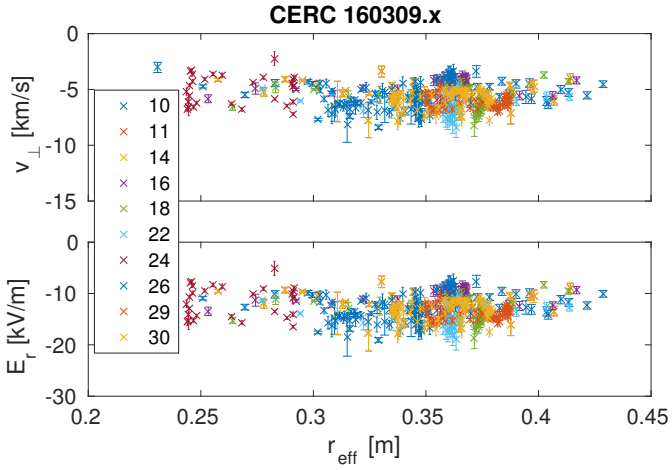

FIG. 6: $v_\perp$ and E_r from the PCR system for the CERC plasmas.

4.3 Influence of position and power on $v_\perp$

For the CERC discharges discussed above the evaluation of $v_\perp$ is done for the frequency range around the carrier frequency of the system of ±350 kHz, only. For the combination of $P_{ECRH} \geq 600\,\mathrm{kW}$ and $r_{eff} \leq 0.25\,\mathrm{m}$ the analysis of $v_\perp$ and E_r yields large error bars in the underlying Δt values. However, the critical density for the probing frequency is still within the plasma. For this cases the cross phase (Φ) spectra is analysed in detail (see fig. 7a,b) for the showcase 160309.24 where the frequency of the reflectometer is set to 32 GHz. For the antenna combination **DE** and the time window $0.66\,\mathrm{s} \leq t \leq 0.69\,\mathrm{s}$, just before the jump in P_{ECRH} from 0.6 MW to 1.3 MW, Φ is characterized by a single negative slope (red dashed line fig. 7a). The slope corresponds well to the broad peak in the coherence (Γ) spectrum as indicated by vertical dashed lines in fig. 7c. In the subsequent time window $0.70\,\mathrm{s} \leq t \leq 0.73\,\mathrm{s}$ a drastic change in Φ and Γ is observed (see fig. 7b,d). The central peak in Γ shrinks in its width. The Φ-spectrum is now characterized

by three slopes. For $-80\,\mathrm{kHz} \leq f \leq 80\,\mathrm{kHz}$ a negative slope for Φ is obtained. And a positive slope in Φ is observed for $80\,\mathrm{kHz} \leq f \leq 190\,\mathrm{kHz}$ and $-190\,\mathrm{kHz} \leq f \leq -80\,\mathrm{kHz}$, respectively. The negative slope corresponds to the central Gaussian in the coherence spectrum representing the propagation of the plasma column (dashed vertical lines in fig. 7b,d) and the positive slopes corresponds to an additional broad peak at $f \approx 160\,\mathrm{kHz}$ representing a propagating turbulent structure. Note, these observations are performed on the same reflection layer and no rotation shear is involved. The measured slopes correspond directly to the velocity according

$$v_\perp(f) = \frac{\Delta z}{d\Phi/df} \tag{4}$$

where Δz denotes the distance between the antenna. The slopes in fig. 7a and those of the high frequency structure in fig. 7b are similar, yielding a similar propagation velocity. The central slope in fig. 7b has a smaller slope and therefore a higher velocity.

The observation is mainly triggered by the applied heating power. Interesting to note that the occurrence of the high frequency mode is related to the ECRH power. The coherence as well as the frequency of the structure is increasing with the P_{ECRH}. The appearance of the structure is not only observed in the CERC plasmas, but, in all plasmas where the heating power is high enough and the reflection layer is localized sufficiently deep in the plasma center. In case of 160308.6 and $t = 1.0\,\mathrm{s}$ with $P_{ECRH} = 3.8\,\mathrm{MW}$ the coherence of the high frequency structure dominates the spectrum. The observation of this high frequency structure could be evidence for the transition from negative to positive E_r which is expected in the plasma center and would be in agreement with the strong power dependence as well.

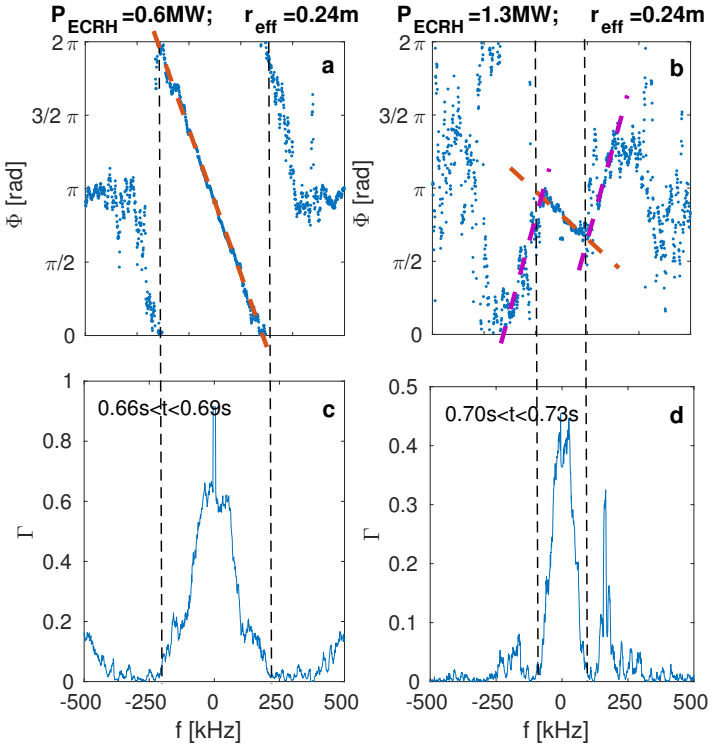

FIG. 7: Crossphase (Φ) and coherence Γ for 160309.24 for two time windows. The coloured dashed lines indicate the slopes in Φ.

5 Summary and Outlook

The poloidal heterodyn correlation reflectometry is successfully installed and commissioned at W7-X. The system is capable to measure turbulence velocities and turbulence properties across a wide radial range in frequency hopping operation. Measurements of the turbulence velocity even outside the last closed flux surface are possible.
Turbulence velocities have been measured for nearly all plasmas in OP1.1. The measured velocity is in the range of $-6\,\mathrm{km\,s^{-1}}$ to $-4\,\mathrm{km\,s^{-1}}$. Neglecting an additional phase velocity, the turbulence velocity is equal to the plasma velocity and the radial electric field can be deduce from the diagnostic. At the last closed flux surface a reversal of the velocity is observed. In the plasma center high frequency structures are observed with a velocity in ion diamagnetic drift direction. Whereas the plasma column yields a negative velocity. This structure increases in the coherence with the applied heating power and with decreasing radius. There may be a connection to the CERC regime which expects a positive velocity and radial electric field in the plasma center.
For the next campaign the system will be upgraded with a second microwave synthesizer to measure radial correlations, too.

References

[1] FUSJISAWA, A., A review of zonal flow experiments, Nucl. Fusion 49 (2009) 013001
[2] HIDALGO, C., Multi-scale physics and transport barriers in fusion plasmas, Plasma Phys. Control. Fusion, 53, (2011), 074003
[3] ESTRADA, T., et al., Experimental observation of coupling between turbulence and sheared flows during L-H transitions in a toroidal plasma, EPL, 92 (2010) 35001
[4] LIANG, Y., et al., Diagnostic set-up and modelling for investigation of synergy between 3D edge physics and plasma-wall interactions on Wendelstein 7-X, IAEA Fusion Energy Conference, Kyoto (2016), Contributed Papers
[5] KRÄMER-FLECKEN, A., et al., Correlation reflectometry at TEXTOR, Rev. Sci. Instrum. 81, (2010), 113502
[6] PASCH, E., et al., First Results from the Thomson Scattering System at the Stellarator Wendelstein 7-X, EPS Conference on Plasma Physics, Leuven (2016), Vol. 40A, P4.016
[7] DREWS, P., et al., Measurement of the plasma edge profiles using the combined probe on W7-X, IAEA Fusion Energy Conference, Kyoto (2016), Contributed Papers
[8] YOKOYAMA, M., et al., Core Electron-Root Confinement (CERC) in Helical Plasmas, Nucl. Fusion, 47, (2007), 1213
[9] DINKLAGE, A., et al., Core Confinement in Wendelstein 7-X Limiter Plasmas, EPS Conference on Plasma Physics, Leuven (2016), Vol. 40A, O2.107
[10] PABLANT, N., et al., Investigation of the Core Radial Electric Field in Wendelstein 7-X Plasmas, EPS Conference on Plasma Physics, Leuven (2016), Vol. 40A, P4.013

Acknowledgement
This work has been carried out within the framework of the EUROfusion Consortium and has received funding from the Euratom research and training programme 2014-2018 under grant agreement No 633053. The views and opinions expressed herein do not necessarily reflect those of the European Commission.